JOURNAL OF MATERIALS SCIENCE 15 (1980) 1568–1576

# Origin of strength anisotropy in hot-pressed silicon nitride

J. E. WESTON
*Department of Metallurgy and Materials Science, University of Cambridge, Pembroke Street, Cambridge, UK*

Three- and four-point room-temperature bend tests were carried out on specimens of a hot-pressed silicon nitride oriented parallel and perpendicular to the hot-pressing direction. Scanning electron microscopy was used to identify and measure the fracture-initating flaws, thus enabling the fracture toughness to be calculated. The strength anisotropy exhibited by this material was attributed to variation in the severity of the inherent flaws in the material with orientation, with the fracture toughness showing no significant anisotropy in this case.

## 1. Introduction

Hot-pressed silicon nitride is usually prepared from a powder containing a high proportion of the $\alpha$-silicon nitride phase, producing a material with improved mechanical properties [1, 2]. However, this type of material also displays anisotropy of its mechanical properties [1, 3, 4].

Lange [1] found that the room-temperature flexural strength of bar specimens cut with their long axes perpendicular to the hot-pressing direction was ~25% greater than that of similar specimens cut with their long axes parallel to this direction. Lange attributed this strength anisotropy to the development during hot-pressing of elongated, lath-like grains of $\beta$-silicon nitride in the material, which show a tendency to be oriented so that the $\beta$-silicon nitride $c$-axis is perpendicular to the hot-pressing direction. This oriented microstructure would then have a greater fracture surface energy ($\gamma_f$) for cracks travelling parallel to the hot-pressing direction than for fractures perpendicular to this direction. This view is supported by Lange's measurements of $\gamma_f$ using double-cantilever beam (DCB) specimens cut so that the crack plane was parallel or perpendicular to the hot-pressing direction [1], although the results were not conclusive. Subsequently, Bansal [3] has used notched beam (NB) specimens to measure the variation of $\gamma_f$ with orientation for a material with a 1 to 2 $\mu$m grain size and has found that $\gamma_f$ is approximately 45% greater when the crack plane is parallel to the hot-pressing direction. This orientation resulted in fully intergranular fracture, while cracks propagating perpendicular to the hot-pressing direction produced 50% transgranular fracture.

An alternative explanation of the anisotropy in these materials has been proposed by Kossowsky [4]. He considered that the relatively small amount of grain orientation resulting from hot-pressing was not sufficient to explain the strength anisotropy displayed by his material. A combination of factors seemed to be involved; i.e. grain orientation plus variations in density perpendicular to the hot-pressing direction plus the presence of anisotropic inclusions. In fact, anisotropic inclusions acted as the fracture initiating flaws in Kossowsky's material. Also, in recent years [5–8], doubt has been expressed regarding the use of fracture parameters found using specimens containing large, pre-existing notches or cracks (e.g. DCB, NB) for the interpretation of the fracture of a material from relatively small inherent flaws, where local inhomogeneities in the microstructure are likely to be of prime importance.

In an attempt to clarify the situation, it was decided to investigate the antisotropy of the fracture behaviour of a relatively pure hot-pressed silicon nitride material, which contains few or no inclusions [9], using fractographic analysis to determine the fracture-initiating flaws for fracture parallel and perpendicular to the hot-pressing direction.


0022–2461/80/061568–09$02.90/0 

## 2. Experimental details

### 2.1 Materials

The material used in this investigation was hot-pressed silicon nitride which was prepared from a high $\alpha$-phase powder using only a small amount of hot-pressing additive*. This method produced a final material with a relatively low proportion of glassy grain-boundary phase and hence an improved creep resistance at elevated temperatures [9].

In order to avoid billet-to-billet variations, all the specimens used in this study were cut from a single billet which had an average density of 3.08 Mg $m^{-3}$ (i.e. 97% theoretical density).

### 2.2. X-ray analysis

A standard X-ray diffractometer employing $CuK_\alpha$ radiation with a 1° colimating slit, a 0.2° receiving slit and a scanning rate of ½°2$\theta$ $min^{-1}$ was used to obtain diffraction traces from the faces of polycrystalline blocks of the material which were oriented parallel or perpendicular to the hot-pressing direction. A powder sample of the hot-pressed material was also analysed using the X-ray diffractometer under similar conditions.

### 2.3. Mechanical testing

Three types of rectangular bar specimen were tested in this study:

(a) type 1: 3 mm x 3 mm x 60 mm specimen long axis perpendicular to hot-pressing direction;

(b) type 2: 3 mm x 3 mm x 30 mm specimen long axis perpendicular to hot-pressing direction;

(c) type 3: 3 mm x 3 mm x 30 mm specimen long axis parallel to hot-pressing direction.

The four large faces of each specimen were diamond-ground parallel to the specimen long axis and the long edges were rounded off on 600 grade silicon carbide abrasive to minimize fracture from edge chips during testing.

Ten specimens of type 1 and twenty specimens each of types 2 and 3 were tested in three-point bending at room temperature. The three-point bend apparatus rested on a 100 kg compression load cell in a standard Instron testing machine. Load was applied to the specimen via the upper knife-edge, which was driven by the Instron cross-head. This knife-edge was free to rotate about an axis perpendicular to the specimen long axis, thus minimizing parasitic stresses in the specimen. The lower knife-edges could be adjusted to obtain span lengths up to 52 mm. All the knife-edges were made of hardened steel and their bearing surfaces were ground with 600 grade silicon carbide abrasive to minimize friction effects during loading. The type 1 specimens were tested with a span of 51.1 mm and type 2 and 3 specimens with a span of 25.3 mm. In all cases the Instron cross-head speed was 0.5 mm $min^{-1}$.

The failure stress of each specimen was calculated using:

$$\sigma_f = \frac{3}{2}\frac{WL}{xy^2} \quad (1)$$

where $\sigma_f$ = fracture stress (N $m^{-2}$), $W$ = load at fracture (N), $L$ = span of lower knife-edges (m), $x(y)$ = specimen width (depth) (m).

Ten specimens of type 1 were tested in four-point bending at room temperature. The apparatus was the same as that used for three-point bend testing, with the upper knife-edge replaced by a double knife-edge of fixed span. The specimens were tested in quarter-point loading, with an outer span of 40.0 mm and an inner span of 20.0 mm, and at a cross-head speed of 0.5 mm $min^{-1}$.

The failure stress of each specimen was calculated using:

$$\sigma_f = \frac{3\,WD}{xy^2} \quad (2)$$

where $D$ = length of moment arm (distance between outer and inner knife-edge) (m).

All the specimens tested failed within the inner span, and hence gave valid results.

### 2.2. Fractography

The fracture surfaces of several specimens of each type were examined by scanning electron microscopy, using a Cambridge Stereoscan II microscope and gold-coated specimens. Both fracture surfaces were examined in each case so that the fracture-initiating flaws could be unambiguously identified. The size of each flaw was measured to allow the critical stress intensity factor ($K_{IC}$) for failure to be evaluated, using a method [10] which takes account of the flaw shape as well as its depth in assessing the severity of the flaw (Fig. 1).

The equation used to calculate $K_{IC}$ was

$$\sigma_f' \approx \frac{1.68}{Y}\left(\frac{K_{IC}}{A^{1/4}}\right), \quad (3)$$

*Rolls Royce Ltd, Aero Division, Derby, UK

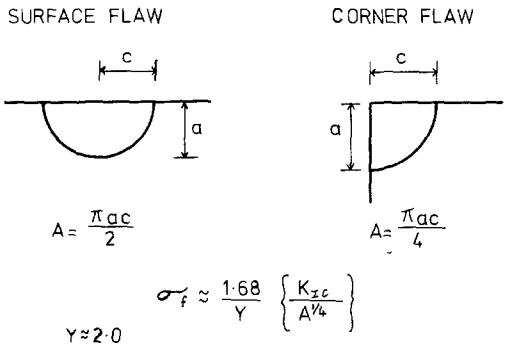


*Figure 1* Measurement scheme for fracture initiating flaws (After [10]).

where $\sigma_f'$ = fracture stress at site of flaw (MN $m^{-2}$), $A$ = flaw area ($m^2$), $Y$ = geometrical parameter [11].

The maximum error in the use of this approximate equation is estimated [10] at 5% for

$$0.2 < a/c < 3.0, \quad (4)$$

where $a$ and $c$ are the semi-axes of the elliptical flaw, as shown in Fig. 1.

For specimens tested in three-point bending, and failing from surface flaws, $\sigma_f'$ can be found from the failure stress ($\sigma_f$), the span ($L$) and the distance ($d$) from the fracture origin to the mid-point (upper knife-edge) position on the specimen:

$$\sigma_f' = \sigma_f \cdot \frac{L - 2d}{L}. \quad (5)$$

## 3. Results

### 3.1 X-ray analysis

X-ray analysis of the hot-pressed silicon nitride showed only the diffraction pattern of β-silicon nitride with no detectable minor phases.

The peak–height ratios for the polycrystalline and powder samples are given in Table I. Examination of the results from the polycrystalline specimens reveals that the peaks from crystal lattice planes intersecting the $c$-axis are suppressed in the trace from the specimen oriented perpendicular to the hot-pressing direction. This indicates that the β-silicon nitride $c$-axis tends to be oriented perpendicular to the hot-pressing direction. This effect has been noted previously [1, 12, 13].

### 3.3. Mechanical testing

Table II is a summary of the results of the mechanical tests carried out in this study.

TABLE I Peak-height ratios from X-ray diffractometer traces of polycrystalline and powder specimens of hot-pressed silicon nitride

| $d$(Å) | $h\,k\,l$ | $I/I_1$ (powder diffraction file) | Polycrystalline surfaces | | Powder sample $I/I$ max |
|---|---|---|---|---|---|
| | | | ∥ H–P axis $I/I$ max | ⊥ H–P axis $I/I$ max | |
| 6.63 | 1 0 0 | 17 | 22 | 48 | 31 |
| 3.82 | 1 1 0 | 20 | 25 | 42 | 39 |
| 3.31 | 2 0 0 | 85 | 59 | 100 | 100 |
| $2.66_8$ | 1 0 1 | 100 | 100 | 44 | 89 |
| $2.49_2$ | 2 1 0 | 100 | 50 | 85 | 94 |
| $2.31_2$ | 1 1 1 | 9 | 9 | 6 | 10 |
| $2.18_0$ | 2 0 1 | 35 | 41 | 13 | 31 |
| $1.90_4$ | 2 2 0 | 5 | 3 | 4 | 7 |
| $1.89_2$ | 2 1 1 | 5 | | | |
| $1.82_7$ | 3 1 0 | 20 | 47 | 15 | 13 |
| $1.75_3$ | 3 0 1 | 70 | 78 | 25 | 40 |
| $1.59_3$ | 2 2 1 | 20 | 12 | 10 | 13 |
| $1.54_8$ | 3 1 1 | 9 | 3 | 4 | 7 |
| $1.51_2$ | 3 2 0 | 35 | 9 | 12 | 17 |
| $1.45_5$ | 0 0 2 | 35 | 16 | 4 | 16 |
| $1.43_7$ | 4 1 0 | 20 | 6 | 10 | 7 |
| $1.35_8$ | 1 1 2 | 3 | – | – | – |
| $1.34_1$ | 3 2 1 | 40 | 25 | 23 | 35 |
| $1.33_0$ | 2 0 2 | 17 | 9 | 4 | 5 |
| $1.31_7$ | 5 0 0 | 17 | – | 6 | 6 |
| $1.28_8$ | 4 1 1 | 85 | 12 | 10 | 20 |
| $1.26_8$ | 3 3 0 | 20 | – | 6 | 7 |
| $1.25_5$ | 2 1 2 | 85 | 12 | 10 | 17 |

TABLE II Results of mechanical tests

| Specimen type | Orientation w.r.t. specimen long axis | Number of tests | Mean fracture stress (MN m$^{-2}$) | Standard deviation (MN m$^{-2}$) | Weibull modulus ($m$) |
|---|---|---|---|---|---|
| Type 1 3-point bend | ⊥ hot-press axis | 10 | 336 | 16 | – |
| Type 1 4-point bend | ⊥ hot-press axis | 10 | 310 | 24 | – |
| Type 2 3-point bend | ⊥ hot-press axis | 20 | 367 | 30 | 14.0 |
| Type 3 3-point bend | ∥ hot-press axis | 20 | 266 | 19 | 15.7 |

Graphs were plotted of probability of failure ($P_f$) versus fracture stress ($\sigma_f$) for the three-point bend tests on type 2 and 3 specimens (Fig. 2). Also, for these specimens, graphs were plotted of $\ln \ln (1/1-P_f)$ versus $\ln \sigma_f$ (Fig. 3). A best straight line fit of the data points in each case was used to find the slope, which is equal to the Weibull modulus ($m$) of the material [14]. The values of $m$ were similar for both types of specimen; type 2: $m = 14.0$, ($\pm$ 3.2), type 3: $m = 15.7$ ($\pm$ 3.6).

From Table II it can be seen that the type 3 specimen had approximately three-quarters of the fracture strength of the type 2 specimens, thus confirming the strength anisotropy which has previously been found in this type of material [1, 4]. However, the strength values for all types of specimen were lower that the usual flexural failure strength of commercial hot-pressed silicon nitride, i.e. approximately 700 to 1000 MN m$^{-2}$ [15].

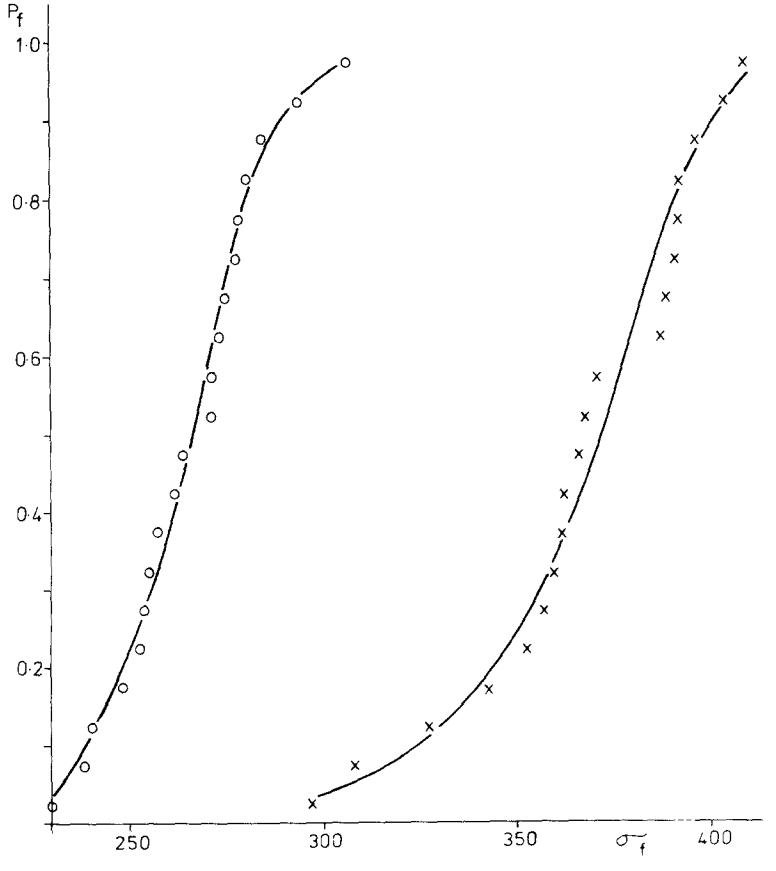


*Figure 2* Plot of probability of failure ($P_f$) versus three-point strength ($\sigma_f$): X = type 2 specimens, O = type 3 specimens.

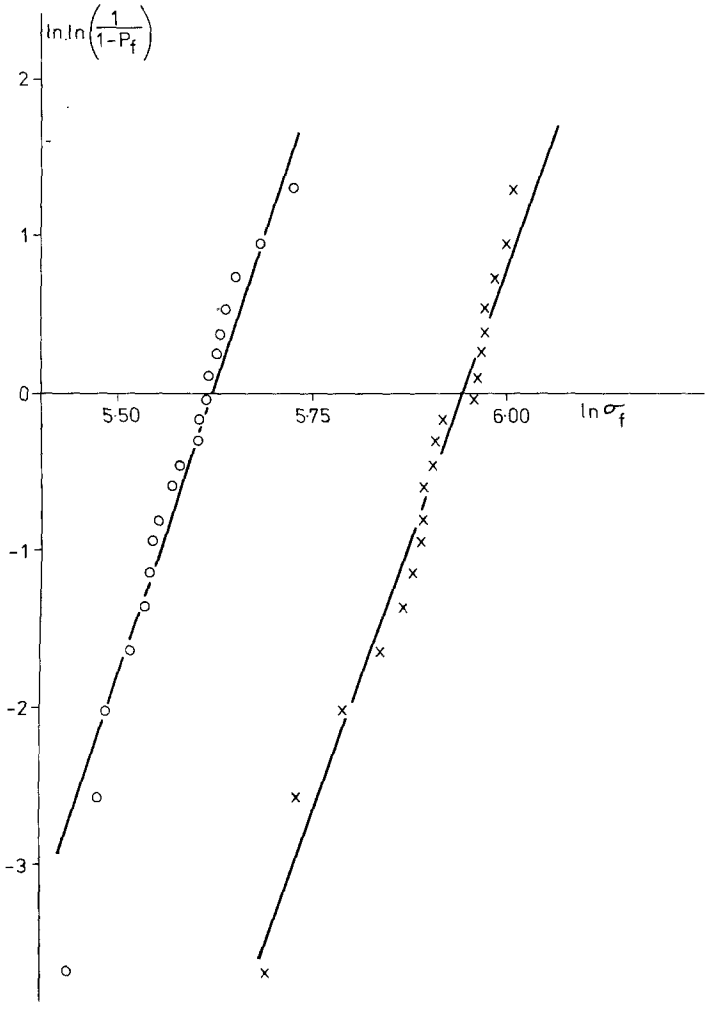


*Figure 3* Plot of $\ln \ln (1/(1-P_f))$ versus $\ln \sigma_f$: X = type 2 specimens, slope = $m = 14.0$, O = type 3 specimens, slope = $m = 15.7$.

## 3.3. Fractography

Scanning electron fractography revealed that the material consisted mainly of relatively large, acicular grains clearly exhibiting a hexagonal habit (Fig. 4). These grains were up to 30 $\mu$m long, with an aspect ratio of approximately 5:1.

The fracture surfaces examined showed poorly defined fracture mirrors which facilitated the identification of the fracture-initiating flaws. In all cases fracture was initiated at or very near (within 50 $\mu$m) the tensile surface of the specimen. It was found that there was a significant difference in the type and size of the fracture-initiating flaws depending on the type of specimen examined (Fig. 5), Table III. The flaws in specimens oriented with their long axes perpendicular to the hot-pressing direction (types 1 and 2) consisted of either approximately semicircular flaws at the tensile surface or at the corner of this surface (Fig. 5a) or elliptical regions of incompletely densified material (Fig. 5b). In both cases the area of the flaw was in the range of 3 to 8 $\times 10^{-9}$ m$^2$. In contrast, the flaws in specimens oriented parallel to the hot-pressing direction (type 3) were relatively large regions of low-density material. with flaw areas in the range of 30 to 60 $\times 10^{-9}$ m$^2$, (Figs. 5c and d).

The $K_{IC}$ values for various specimens tested in three-point bending were calculated from the measured flaw sizes using Equations 3 and 5 (Table III). The mean value of $K_{IC}$ for specimens of types 1 and 2 (perpendicular to the hot-pressing direction) was $3.5 \pm 0.5$ MN m$^{-3/2}$ and the mean value for type 3 specimens (parallel to the hot-pressing direction) was $4.3 \pm 0.5$ MN m$^{-3/2}$. These values are similar to the results found by other workers using similar techniques on commercial hot-pressed silicon nitrides [16].

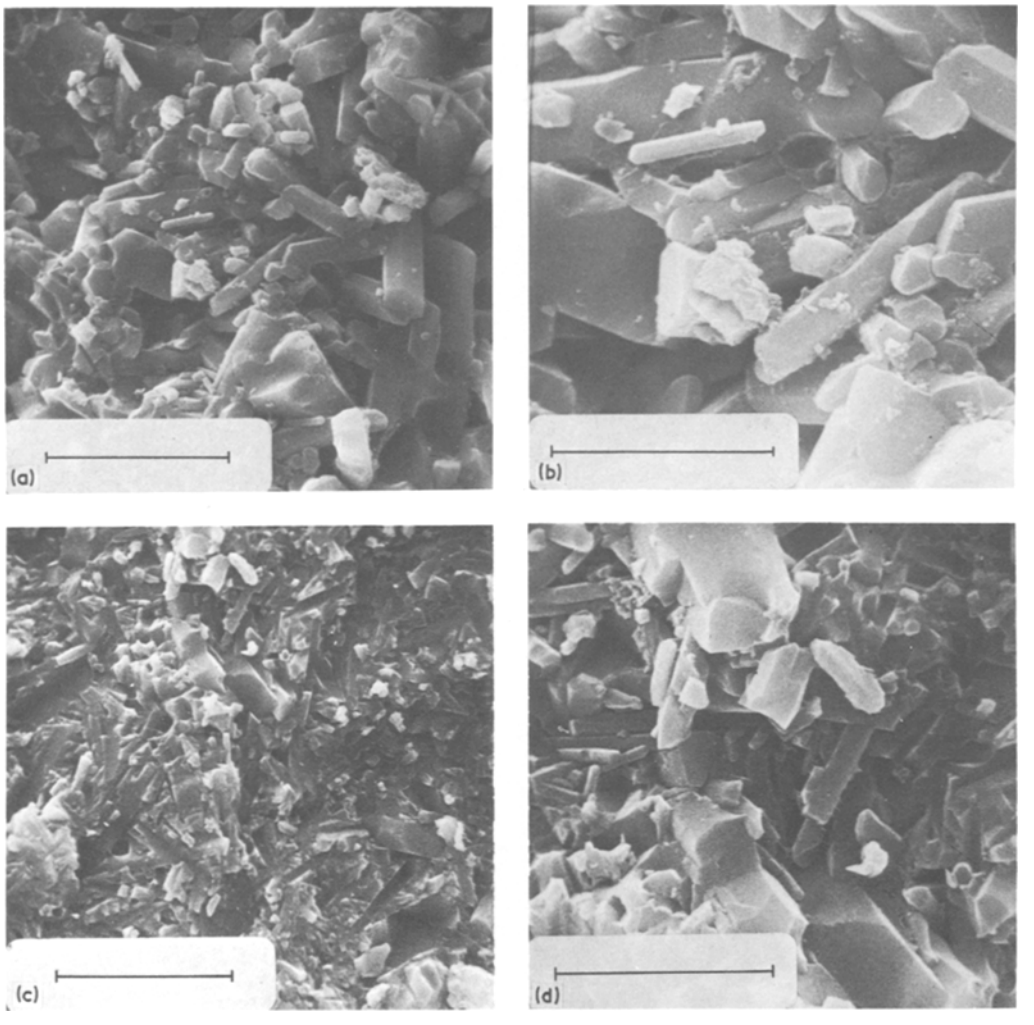


*Figure 4* Typical fracture surfaces in three-point bend tests. (a) Type 2 specimen, bar = 15 $\mu$m, (b) Detail of (a), bar = 7.5 $\mu$m, (c), Type 3 specimen, bar = 15 $\mu$m, (d) Detail of (c), bar = 7.5 $\mu$m.

TABLE III Calculation of $K_{IC}$ from flaw-size measurements

| Specimen type | Flaw type* | $a$ ($\mu$m) | $c$ ($\mu$m) | $a/c$ | $A$ ($10^{-9}$ m$^2$) | $\sigma_f'$ at flaw site (MN m$^{-2}$) | $K_{IC}$ (MN m$^{-3/2}$) |
|---|---|---|---|---|---|---|---|
| 1 | C | 97 | 97 | 1.0 | 7.4 | 297 | 3.3 |
| 1 | S | 66 | 35 | 1.9 | 3.6 | 340 | 3.1 |
| 2 | S | 46 | 78 | 0.6 | 5.7 | 329 | 3.4 |
| 2 | C | 93 | 93 | 1.0 | 6.8 | 356 | 3.8 |
| 2 | S | 102 | 36 | 2.8 | 5.8 | 301 | 3.1 |
| 2 | S | 54 | 66 | 0.8 | 5.6 | 391 | 4.0 |
| 2 | S | 37 | 74 | 0.5 | 4.3 | 377 | 3.6 |
| 3 | S | 163 | 209 | 0.8 | 53.5 | 236 | 4.3 |
| 3 | C | 202 | 243 | 0.8 | 38.5 | 229 | 3.8 |
| 3 | C | 223 | 223 | 1.0 | 39.2 | 252 | 4.2 |
| 3 | S | 116 | 116 | 1.0 | 21.2 | 306 | 4.4 |
| 3 | S | 182 | 182 | 1.0 | 52.0 | 259 | 4.7 |

*S = Surface flaw C = Corner flaw

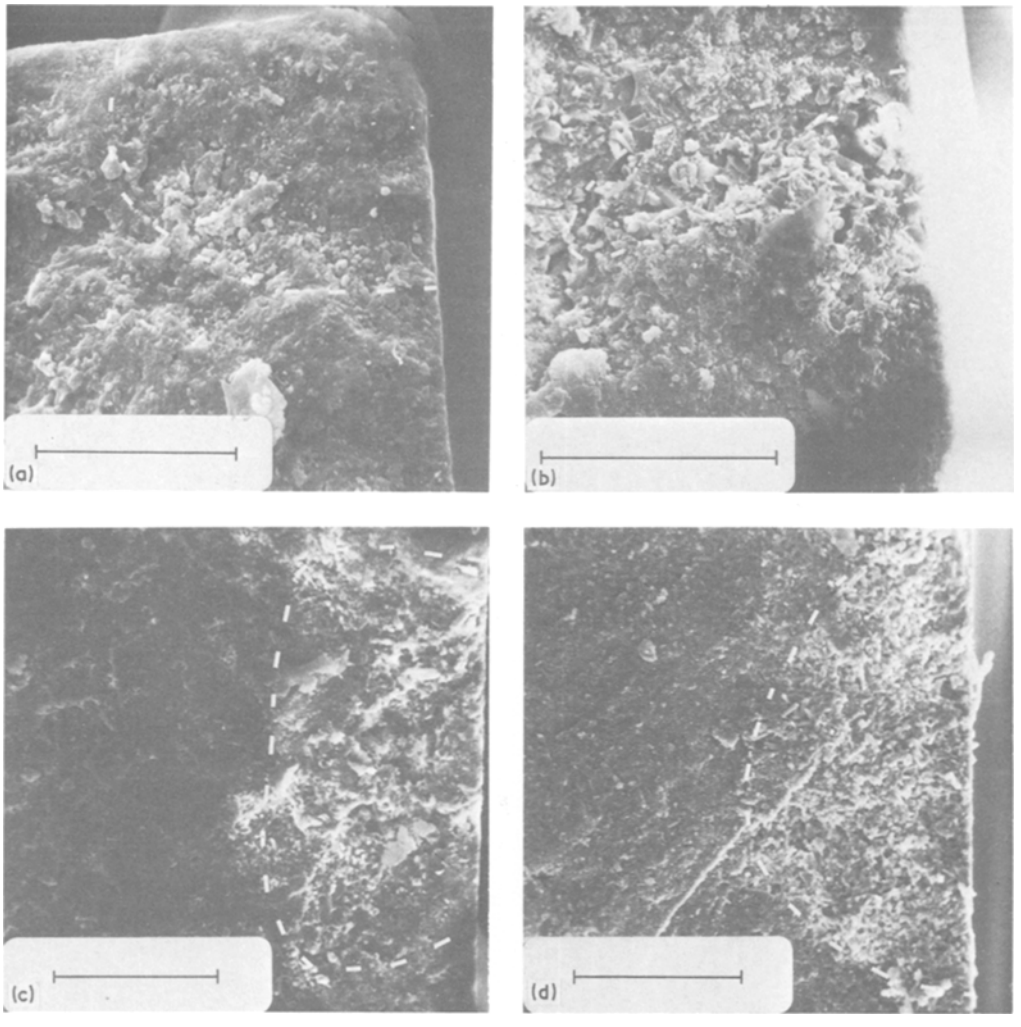


*Figure 5* Typical fracture-initiating flaws in three-point bend test, (approximate flaw periphery outlined). (a) Type 1 specimen, bar = 75 $\mu$m; flaw area = $7.4 \times 10^{-9}$ m$^2$. (b) Type 2 specimen, bar = 75 $\mu$m; flaw area = $5.8 \times 10^{-9}$ m$^2$. (c) Type 3 specimen, bar = 150 $\mu$m; flaw area = $53.5 \times 10^{-9}$ m$^2$. (d) Type 3 specimen, bar = 150 $\mu$m; flaw area = $52.0 \times 10^{-9}$ m$^2$.

Detailed examination of the fracture surfaces of specimens remote from the site of initiation revealed that the specimens with their long axes perpendicular to the hot-pressing direction exhibited predominantly intergranular failure (Fig. 4a and b), while specimens oriented parallel to the hot-pressing direction exhibited mixed intergranular and transgranular failure (Fig. 4c and d).

## 4. Discussion

The relatively low fracture strengths of the material investigated here are probably a result of its composition and its preparation schedule. This material was designed to contain a small amount of grain-boundary phase to reduce creep at high temperature [9]. Thus the material would have contained only a small amount of liquid phase at the hot-pressing temperature so that the densification rate was slow and a prolonged interval at the hot-pressing temperature was required to obtain a satisfactory final density. This process had three important consequences for the material's strength:

(a) incomplete densification, so that the final material contained regions of low density;

(b) relatively weak inter-grain bonding, due to the low concentration of bonding phase;

(c) pronounced grain growth of the $\beta$-silicon

nitride grains formed at the hot-pressing temperature*.

Incomplete densification leading to the formation of anisotropic regions of low density in the hot-pressed product is clearly indicated by the fracture-initiating flaws in the specimens oriented such that the fracture plane was perpendicular to the hot-pressing direction. As the pressure applied during hot-pressing was uni-axial, the low-density regions in the product were in the form of discs with their smallest dimension parallel to the hot-pressing direction. Thus these regions acted as the mose severe flaws in specimens where the fracture plane was parallel with their large dimensions, i.e. type 3 specimens in this study. This observation supports the proposal by Kossowsky [4] that the strength anisotropy of hot-pressed silicon nitride is not solely due to the orientation of the $\beta$-silicon nitride grains.

As $\beta$-silicon nitride is hexagonal, and hence exhibits anisotropic thermal expansion, the large grain size in this material would accentuate the thermal anisotropy stresses across the grain boundaries. This effect, coupled with relatively weak grain-boundary bonding, may lead to a material susceptible to the formation of surface cracks during machining. Such crack formation may be due to thermal shock during machining or the superposition of machining stresses on residual stresses present in the specimen, formed during cooling from the hot-pressing temperature. This interpretation is supported by the observation of fracture-initiating flaws which appear to be due to machining damage in specimens oriented perpendicular to the hot-pressing direction (types 1 and 2).

In the light of the observed differences in fracture-initiating flaws in type 2 and 3 specimens, it is probably fortuitous that these two types of specimen produced similar values for the Weibull modulus ($m$). However, considering specimens oriented with their long axes perpendicular to the hot-pressing direction only, the value of $m$ found for the smaller type 2 specimens in three-point bending can be used to predict the ratio of the mean fracture strengths between the type 2 specimens and the larger type 1 specimens in three-point and four-point bending [17] (Table IV). The reasonably good agreement obtained for the measured and calculated mean strength ratios indicates that the same population of flaws is responsible for failure in all the specimens oriented perpendicular to the hot-pressing direction.

TABLE IV Comparison of ratios of mean fracture stresses with ratios calculated for specimens oriented perpendicular to the hot-pressing axis ($m = 14.0$)

| | | $\left\{\frac{\bar{\sigma}_1}{\bar{\sigma}_2}\right\}$ calc | $\left\{\frac{\bar{\sigma}_1}{\bar{\sigma}_2}\right\}$ obs |
|---|---|---|---|
| Type 2: (3-point) | type 1 (3-point) | 1.05 | 1.09 |
| Type 2: (3-point) | type 1 (4-point) | 1.20 | 1.18 |
| Type 1: (3-point) | type 1 (4-point) | 1.14 | 1.09 |

In contrast to the fracture energy measurements of Lange and Bansal [1, 3], the values of $K_{IC}$ measured here were similar for specimens parallel and perpendicular to the hot-pressing direction. However, both Lange and Bansal used specimens (NB or DCB) containing large, pre-existing flaws so that their results gave an average value of the fracture energy, while in this investigation the local value of $K_{IC}$ in the region of the fracture-initiating flaw was measured. The examination of the fracture surfaces shows that, remote from the fracture-initiation site, the fracture mode is predominantly intergranular for cracks travelling on planes parallel to the hot-pressing direction and a mixture of intergranular and transgranular fracture for cracks travelling on planes perpendicular to this direction. This is in agreement with the observations of Bansal [3] and suggests that there would be anisotropy in the average fracture mechanics parameters of the material studied here.

The similarity of the local $K_{IC}$ values for the two specimen orientations suggests that in both cases fracture is predominantly intergranular in close proximity to the fracture-initiating flaw. For the specimens oriented parallel (fracture plane perpendicular) to the hot-pressing direction this would mean that fracture was originally intergranular and then changed to mixed-mode failure as fracture

*Although many grains showed the elongated prism morphology more usually associated with large additions of hot-pressing additives, it was noted that this effect was most pronounced in low-density regions where individual grains could grow to a large size without impingement from neighbouring particles. Therefore, the well-developed grain morphology in this material was probably due to its relatively low density (97% theroretical) and prolonged heat-treatment.

proceeded. This may be due to the nature of the fracture-initiating flaws in this case, i.e. low-density regions where there is reduced orientation of the acicular β-silicon nitride grains, thus favouring intergranular failure. Thus for both specimen orientations, the fracture toughness value for fracture initiation is similar and the strength anisotropy is due to the differences in the size and type of the fracture-initiating flaws.

The $K_{IC}$ values found for the material studied here are similar to those for commercial hot-pressed silicon nitrides [16], although this material contains less grain-boundary phase. Thus this material probably has weaker grain boundaries and so should have a lower value of $K_{IC}$ for intergranular failure. However, the large grain size and well developed acicular habit of the β-silicon nitride grains leads to a very rough fracture surface with grain pull-out of the fibrous grains (Fig. 4a and b). The large fracture surface-area produced and the energy absorbed in grain pull-out tend to increase the fracture toughness of the material and so counteract the weaker grain-boundary bonding.

## 5. Conclusions

(1) The hot-pressed silicon nitride studied here exhibited strength anisotropy although there was no significant variation with orientation in the value of $K_{IC}$ found from the size of the fracture-initiating flaws. Thus this strength anisotropy was due to the variation in the severity of the inherent flaws on the fracture plane in the material, depending on the orientation of this fracture plane with respect to the hot-pressing direction.

(2) Fractographic evidence suggests that there is a change in fracture mode for cracks propagating perpendicular to the hot-pressing axis, i.e. intergranular fracture in the vicinity of the fracture-initiating flaw, changing to mixed-mode fracture remote from this flaw. Fracture on planes parallel to the hot-pressing direction is always predominantly intergranular. This may explain the anisotropy in fracture energy found by previous workers using specimens containing large, pre-existing cracks.


## Acknowledgements

The author is grateful both to Mr J. Bird of Rolls Royce Ltd, Aero Division, Derby, who supplied the specimens used in this study and to Professor R. W. K. Honeycombe for the provision of experimental facilities in the Department of Metallurgy and Materials Science, University of Cambridge.


## References


1. F. F. LANGE, *J. Amer, Ceram. Soc.* **56** (1973) 518.
2. L. J. BOWEN and T. G. CARRUTHERS, *J. Mater. Sci.* **13** (1978) 684.
3. G. K. BANSAL, in "Ceramic Microstructures 76", edited by R. M. Fulrath and J. A. Pask (Westview Press, Berkeley, 1977). p. 860.
4. R. KOSSOWSKY, *J. Mater. Sci.* 8 (1973) 1603.
5. A. G. EVANS, in "Fracture Mechanics of Ceramics", Vol. 1, edited by R. C. Bradt, D. P. H. Hasselman and F. F. Lange (Plenum Press, New York, 1974) p. 17.
6. R. W. RICE, *ibid* Vol. 1, p. 323.
7. S. W. FREIMAN, K. R. MCKINNEY and H. L. SMITH, *ibid* Vol. 2, p. 659.
8. S. W. FREIMAN, A. WILLIAMS, J. J. MECHOLSKY and R. W. RICE, in "Ceramic Microstructures 76", edited by R. M. Fulrath and J. A. Pask (Westview Press, Berkeley, 1977) p. 824.
9. J. BIRD, Rolls Royce Ltd, Private communication.
10. G. K. BANSAL, *J. Amer. Ceram. Soc.* **59** (1976) 87.
11. W. F. BROWN, JR and J. E. SRAWLEY, ASTM Special Technical Publication, No. 410 (1967) p. 1.
12. J. E. WESTON, P. L. PRATT and B. C. H. STEELE, *J. Mater. Sci.* **13** (1978) 2137.
13. K. NUTTALL and D. P. THOMPSON, *ibid* **9** (1974) 850.
14. K. TRUSTRUM and A. DE. S. JAYATILAKA, *ibid* **14** (1979) 1080.
15. J. W. EDINGTON, D. J. ROWCLIFFE and J. L. HENSHALL, *Powder Met. Int.* 7 (1975) 82.
16. *Idem, ibid* 7 (1975) 136.
17. D. G. S. DAVIES, *Proc. Brit. Ceram. Soc.* **22** (1973) 429.


Received 13 September and accepted 13 November 1979.